Progress In Electromagnetics Research M, Vol. 49, 21–31, 2016

The Performance Improvement of THz Antenna via Modeling and Characterization of Doped Graphene

Mohammed Taih Gatte[1, 2, *], Ping Jack Soh[1], Hasliza A. Rahim[1], R. Badlishah Ahmad[1], and MohamedFareq AbdulMalek[3]

Abstract—The improvement of Terahertz (THz) antenna requires efficient (nano)materials to operate within the millimeter wave and THz spectrum. In this paper, doped graphene is used to improve the performance of two types of patch antennas, a rectangular and an elliptical antenna. The surface conductivity of conventional (non-doped) graphene is first modeled prior to the design and simulation of the two graphene based antennas in an electromagnetic solver. Next, different graphene models and their corresponding surface conductivities are computed based on different bias voltages or chemical doping. These configurations are then benchmarked against a similar antenna based on conventional metallic (copper) conductor to quantify their levels of performance improvement. The graphene based antennas showed significant improvements for most parameters of antenna than that of the conventional antenna. Besides that, the higher chemical potentials resulting from higher biasing voltages also resulted in this trend. Finally, the elliptical patch graphene antenna indicated better reflection performance, radiation efficiency and gain than a rectangular patch operating at the same resonant frequency.

1. INTRODUCTION

The crowding increasing of wireless communications spectrum and demands for bandwidths have resulted in the exploitation of millimetre-wave (mm-wave) and TeraHertz (THz) bands potentially for applications such as imaging, spectroscopy, sensing and detection [1]. Since most materials absorb THz radiation, THz signals detected using an antenna may be used in molecular spectroscopy or fingerprint detection in sensing explosives, drugs, chemical and biological weapons. The limited range due to high path loss and low receiver sensitivity requires the available incident power at a detector to be maximized using an efficient antenna.

Development of THz antennas is relatively recent [2]. Besides considering their efficiency improvements from the perspective of electromagnetism, understanding their physical and materials science aspects is also crucial [3]. THz antennas must be efficient to ensure high gain, besides being wideband, miniaturized in size and cost effective. Photoconductive antennas have been suggested for such applications. However, the often poor impedance matching between these antennas and their photomixers often leads to the degradation of antenna efficiency. An alternative to overcome this drawback is to utilize microstrip patch antennas [4]. Several previous studies have investigated THz microstrip antennas' substrates, while others investigated its conductive elements [5] such as gold and platinum. Their common use as conducting materials in the mm-wave and THz frequency bands is due to their high conductivity and antioxidization behavior in air [6]. However, metals are typically lower in conductivity in the THz frequencies than in DC or microwaves. This leads to increased penetration

Received 4 May 2016, Accepted 7 June 2016, Scheduled 10 July 2016

* Corresponding author: Mohammed Taih Gatte (mohtaih@gmail.com).

[1] University Malaysia Perlis, Perlis, Malaysia. [2] Ministry of Science and Technology, Iraq. [3] University of Wollongong in Dubai, Dubai, UAE.

of field in metals, high surface resistance and consequently, degradation of the radiation efficiency in metallic THz antennas [7, 8]. On the contrary, metallic thin film may be prone to micro-cracks [9].

Nanomaterials such as graphene and Carbon Nanotubes (CNTs) are suitable options to overcome metallic losses in these applications. For example, the resistivity of a single wall (SW) CNT is lower than that of a strand gold with the same diameter, making it a major motivating factor in utilizing CNTs for fabricating nanoantennas [10, 11]. However, its high (20 kΩ to 10 MΩ) impedance complicates matching between CNT RF devices and other conventional 50 Ω RF devices such as metal multilayers on dielectrics or metal semiconductor heterostructures. Although 50 Ω impedance can be achieved using bundled CNTs, controlling this process is rather complex. On the contrary, graphene, besides its excellent conductivity, also features controllable and tuneable 50 Ω impedance [12]. It is also a promising material for fabricating the wireless communication systems of next generation [13], which require high mobility, low power and broadband operation [14]. Graphene nanoribbon (GNR) can be potentially applied in wireless nano-sensors and devices operating in the THz band [15, 16]. When integrated with flexible dielectric substrates, GNR can also overcome the proneness of micro-cracks in metallic thin films for conformal antennas. For example, a conformal microstrip patch consisting of two parallel electric conductors separated by a dielectric material was proposed in [17], fabricated by thin film deposition and nanolithography techniques [18]. Besides solving the mismatch problems in the THz regime [4], this basic topology is also widely used due to its miniaturization ability and conformality [10]. Meanwhile, an analysis on the surface conductivity of the graphene sheet and the design of a GNR-based patch was discussed in [19]. A graphene-based rectangular microstrip patch THz antenna using a polyimide substrate was presented in [14]. The proposed antenna resonated at 0.75 THz and featured 5.09 dB and 86.58% gain and radiation efficiency, respectively. A transparent graphene antenna was also studied within 5.66 to 6.43 THz band. Its radiation efficiency and gain were found to be 37.17% and 3.27 dB, respectively, at 6 THz resonance [20]. Besides that, quartz substrate was used to design a tuneable triangular graphene-based antenna for operation at 2.60 THz. The resulting gain and radiation efficiency, validated numerically, were 5.97 dB and 82.7% when biased with a 0.5 eV chemical potential [21]. From the literature review, it is validated that graphene exhibits excellent properties in terms of input impedance matching, frequency-configurability, and stable radiation patterns and impedance upon tuning [22].

In this paper, an investigation of the improvements in the level of surface conductivity and impedance via chemical doping or potential biasing is performed. Two different graphene based antennas are studied in terms of radiation efficiency, gain, directivity and reflection coefficient. To achieve this objective, the graphene layer's surface impedance is first modelled numerically based on different doping (biasing). These surface properties are then applied on the two graphene-based antennas: a rectangular and an elliptical patch antenna that fed using microstrip transmission lines. It has been observed that the optimization of the elliptical patch produced a maximum radiation efficiency and gain of 96% and 7.21 dB, respectively, via a 0.5 eV chemical potential. They, by far, are the best values reported in open literature investigated numerically. The organization of the paper is as follows. Section 2 describes the modelling of the frequency-dependent properties of the graphene-based surface conductivity. Next, the parameters are implemented on the proposed antennas in the following section. Besides the surface properties, in this section the effects of the geometrical parameters on the antenna performance in the design and numerical simulation are also studied. The results are presented and discussed in Section 4 prior to some concluding remarks.

2. MODELLING OF COMPLEX SURFACE PROPERTIES OF GRAPHENE

The graphene monolayer is a two-dimensional material composed of carbon atoms bonded in hexagonal structures. It can be represented by an infinite sheet with surface conductivity, which can be modelled via Kubo formula [23].

$$\sigma(\omega) = \sigma_{\text{intra}}(\omega) + \sigma_{\text{inter}}(\omega) \tag{1}$$

It consists of an intraband contribution

$$\sigma_{\text{intra}}\left(\omega, \mu_c, \Gamma, T\right) = \frac{q_e^2 K_B T}{\pi\hbar^2(\omega - j2\Gamma)}\left[\frac{\mu_c}{K_B T} + 2\ln\left(e^{-\mu_c/K_B T} + 1\right)\right] \tag{2}$$

And an interband contribution

$$\sigma_{\text{inter}}(\omega, \mu_c, \tau, T) = \frac{q_e^2}{4\pi\hbar}\left[\frac{2|\mu_c| - (\omega + j\tau^{-1})}{2|\mu_c| + (\omega + j\tau^{-1})}\right] \tag{3}$$

where j is the imaginary unit, q_e the electron charge, $\hbar$ the reduced Plank constant, K_B the Boltzmann's constant, T the temperature, μ_c the chemical potential, and ω the operating angular frequency. Scattering rate $\Gamma = 1/2\tau$ represents its loss mechanism and τ the relaxation time. The value of τ in previous literature ranges between 10^{-11} and 10^{-14} [5]. In this work, the utilized τ is 3×10^{-12} [23, 24]. The two terms of the surface conductivity are calculated using Eqs. (2) and (3). The first term (intraband term) dominates the value of total conductivity in the range of frequency below 5 THz, whereas the second term (interband term) has no significant effect on the total surface conductivity within this band (see Figure 1(a)). Figure 1(b) shows the effect of changing graphene chemical potential μ_c on the surface conductivity. It depends on the carrier density, which can be controlled by gate voltage, electric bias field, or chemical doping. Increasing μ_c leads to the increase in graphene surface conductivity, which shifts antenna resonances to higher frequencies. The shifting of antenna resonance, due to changing μ_c enhances flexibility for the design of tuneable antennas, especially within the THz band. The variation of μ_c enables the resonant frequency tunability feature. Meanwhile, the value of the chemical potential μ_c is electrically controlled by varying the bias voltage (gate voltage, Vg) on the graphene layer. The relation between chemical potential and the bias voltage is explained by the following formula [25].

$$Vg = \left[\frac{q_e \mu_c^2 h}{\pi\hbar^2 v_f^2 \varepsilon_0 \varepsilon_r}\right] \tag{4}$$

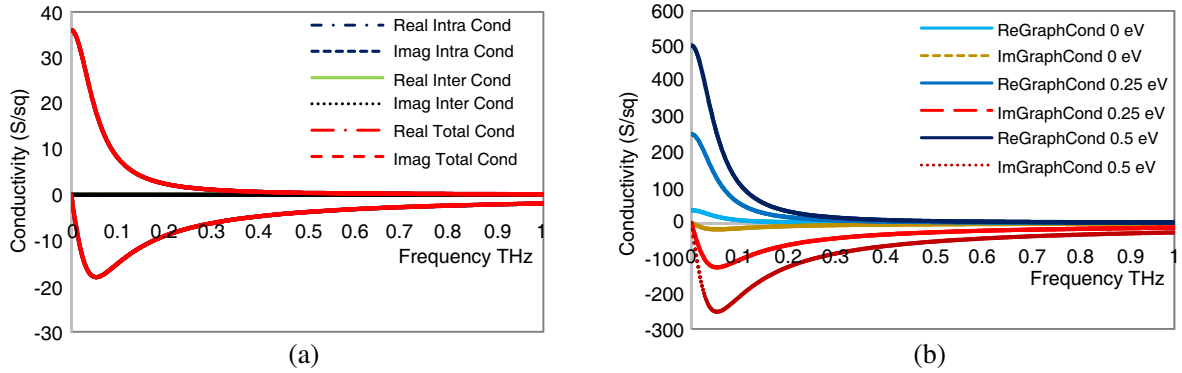

Figure 1. Conductivity of graphene, (a) intra, inter and total conductivity at 0 eV chemical potential, (b) real and imaginary graphene conductivity for different chemical potentials.

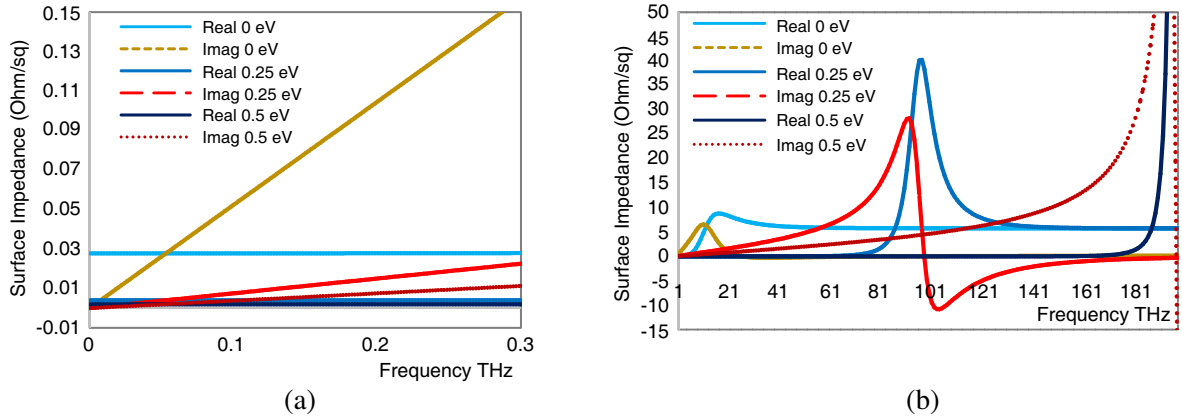

Figure 2. Calculated surface impedance of graphene, (a) in mm-wave band, (b) in THz and infrared band.

where h is the substrate thickness and ε_r the relative permittivity of the substrate. The computation of electromagnetic scattered field from the graphene structure is related to the coupling between the graphene conductivity model and Maxwell's equations.

The main modelling challenge is the assumption of an infinitesimally thin layer of graphene which is discretized by a finite mesh cell size in space for numerical calculation. Graphene sheet is typically modelled based on equivalent surface impedance $Z_s = 1/\sigma$, where σ is frequency dependent surface conductivity computed using Equations (2) and (3). Different values of chemical potentials then result in different graphene models. Figures 2(a) and (b) show the frequency-dependent surface impedance of these models. They are then added to the material library of CST prior to numerical simulation to study the effect of chemical potential variation on the graphene based antenna performance.

3. ANTENNA DESIGN PARAMETERS

In this section, the parameters which affect the configurability of graphene-based antenna are investigated. Two types of parameters are studied. The first is related to the geometric shape whose parameters are controllable by software in numerical simulations. The second parameter is related to the doped graphene model based on the calculation in the previous section. These investigations are necessary in understanding the behaviour of graphene antenna and future study for graphene-based antennas.

3.1. Geometrical Parameters of the Proposed Patch Antennas

The graphene-based microstrip patches antenna depicted in Figure 3 consists of a conducting patch and a feeding line on top of a thin layer of dielectric substrate ($2.2 \leq \varepsilon_r \leq 12$) [17]. The ground plane is placed

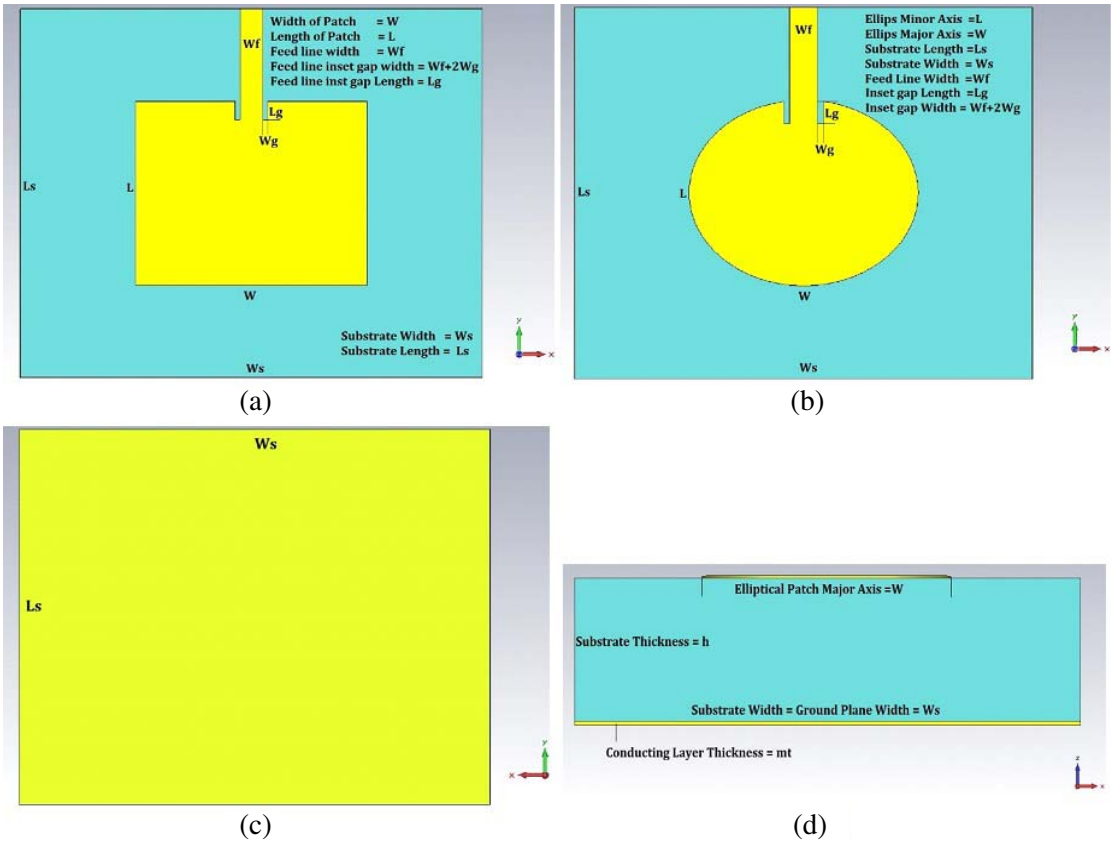

Figure 3. (a) Rectangular patch (front view), (b) elliptical patch (front view), (c) the ground plane located on the reverse side of both antennas and (d) the cross section of both antennas (with the elliptical patch shown as example).

on the bottom of this layer. The conducting patch generally can be designed using different shapes [26]. Two typical microstrip patch antenna topologies are chosen for their simplicity and ease of fabrication: a rectangular-shaped and an elliptical-shaped patch antenna, and both models are used to validate the calculated surface properties in the previous section. The thickness of the thin polyimide substrate, which separates the radiating patch from the ground plane must comply with its traditional limitation of $h \ll \lambda$ and $0.003\lambda_0 \leq h \leq 0.05\lambda$. It is to prohibit the generation of surface waves in the classical metallic patch antennas [17]. To study the geometrical effect on the behaviour of both (rectangular and elliptical) antennas, the width and length of rectangular patch are made equal to the major and minor axes of the elliptical patch, respectively, in a way that both patches are designed with symmetrical dimensions (width and length of the patch, substrate, strip feedline and inset feed gap), which are kept constant for both patches so that satisfactory reflection coefficient will be produced. The differences in shape imply that different surface areas will be produced for different patch antenna types. To design a rectangular patch antenna, the resonant frequency is selected as $f_r = 1.290$ THz, and the thickness of the polyimide substrate is $h = 4\,\mu$m. The other dimensions of the rectangular patch are computed and approximated as listed in Table 1. The rectangular and elliptical patch antennas are simulated over the 0.3 THz to 3 THz frequency band using pure copper as conducting layers and polyimide as its substrate. To simplify the analysis, the dispersion of polyimide substrate is not considered in simulations. It is also the default setting for this particular material in the simulator's library.

The rectangular patch, which will be referred to as Patch1, resonates at 1.291 THz. Meanwhile, the elliptical patch, referred to as Patch2, resonates at 1.488 THz. Next, the major axis of elliptical patch was increased by the ratio of the resonance frequency of both patches f_r (Patch2)$/f_r$ (Patch1) to standardize the resonance of the elliptical patch to that of Patch1 at 1.291 THz. This new elliptical

Table 1. Parameters of the proposed patch antenna.

Parameters	**Symbol**	**Value**
Resonant Frequency	f_r	1.291 THz
Patch width	W	80 μm
Patch Length	L	$W \times 3/4$
Substrate length and width	$Ls \times Ws$	$2 * L \times 2 * W$
Substrate thickness	h	$W/20$
Substrate dielectric constant	ε_r	3.5
Length of the microstrip feed line	Lf	$(L/2 + Lg)$
Width of the microstrip feed line	Wf	$W/10$
Length of the inset gap of the microstrip feed line	Lg	$L/10$
Width of the inset gap of the microstrip feed line	Wg	$Wf/10$

Table 2. Performance comparison of the proposed pure copper based rectangular (Patch1 and Patch4) and elliptical patches (Patch2 and Patch3).

$n = 1$, $Wn = W1 = W = 80\,\mu$m, $L = Wn * 3/4$, $Lg = L/10$, $Wf = (Wn + (W - Wn))/10$, $Wg = Wf/10$, $h = (Wn + (W - Wn))/20$						
	f_r in THz	S_{11} at f_r in −dB	BW at −10 dB in (GHz)	η_{rad} at f_r in (%)	Dir at f_r in dB	Gain at f_r in dB
Patch1	1.291	14.87	28	56.8	7.38	4.92
Patch3	1.291	16.31	28	56.4	7.45	4.93
Patch2	1.488	17.63	34	60.6	7.37	5.2
Patch4	1.488	16.44	33	61	7.33	5.19

patch will be referred to as Patch3. On the other hand, the width of the rectangular patch was decreased by the ratio of f_r (Patch1)/f_r (Patch2) to ensure that the new rectangular patch resonates at the same resonant frequency as of Patch2 at 1.488 THz. This new structure will now be referred to as Patch4. Table 2 shows the simulated results of the four patch antenna models.

3.2. Behavior of the Doped Graphene-Based Patch Antennas

The pure copper metal patch antennas simulated in the previous section are re-simulated using the new calculated doped and non-doped graphene surface properties modeled in Section 2. These calculated values are used to replace the conductivities of the pure copper conducting layers. Three models of graphene are compared with the pure copper model: 0 eV or nondoped graphene (referred to as $G0$), 0.25 eV doped graphene (referred to as $G1$) and 0.5 eV doped graphene (referred to as $G2$). Simulations indicate that there are obvious differences between the performances of the four patch antenna models. Their performance variations in terms of resonant frequency (f_r), reflection coefficient, bandwidth (BW), radiation efficiency (η_{rad}) and gain are summarized in Table 3 and will be explained in the following section.

Table 3. Performance comparison of the proposed rectangular and elliptical patch using copper (pure), non-doped and doped graphene.

$L = Wn * 3/4$, $Lg = L/10$, $Wf = (Wn + (W - Wn)/10$, $Wg = Wf/10$, $h = (Wn + (W - Wn)/20$							
Patch number and design Parameters	Conducter material	f_r in THz	S_{11} at f_r in −dB	BW at −10 dB in GHz	η_{rad} at f_r (%)	Dir at f_r in dB	Gain at f_r in dB
$n = 1$, Patch1	Copper	1.291	14.87	28	56.8	7.38	4.92
$Wn = W1 = W$	$G0$	1.277	27.81	27	76	7.36	6.19
$W1 = 80\,\mu$m	$G1$	1.296	25.35	24	92	7.43	7.07
$f_{r1} = 1.291$ THz	$G2$	1.299	25.11	25	93	7.43	7.09
$n = 3$, $f_{r3} = f_{r1}$	Copper	1.291	16.31	28	56	7.45	4.93
Patch3, $Wn = W3$	$G0$	1.277	38.03	26	78	7.48	6.37
$W3 = W * f_{r2}/f_{r1}$	$G1$	1.299	27.74	21	95	7.44	7.17
$W3 = 92.25\,\mu$m	$G2$	1.3	27.44	21	96	7.46	7.20
$n = 2$, Patch2	Copper	1.488	17.19	34	61	7.38	5.18
$Wn = W2 = W$	$G0$	1.470	32.22	31	81	7.4	6.47
$W2 = 80\,\mu$m	$G1$	1.491	21.2	27	94	7.41	7.18
$f_{r2} = 1.488$ THz	$G2$	1.493	21.1	28	95	7.43	7.21
$n = 4$, $f_{r4} = f_{r2}$	Copper	1.488	16.44	33	61	7.33	5.19
Patch4, $Wn = W4$	$G0$	1.471	29.78	35	80	7.32	6.36
$W4 = W * f_{r1}/f_{r2}$	$G1$	1.493	27.85	32	91	7.39	7.00
$W4 = 69.25\,\mu$m	$G2$	1.496	26.77	32	92	7.39	7.02

4. RESULTS AND DISCUSSION

Table 3 shows the performance of patch antenna when using pure copper, nondoped ($G0$) and doped graphene ($G1$&$G2$) for all conducting layers (patch, strip feed line and ground plane) of four different patches mentioned in the previous section. The pure copper based patch antenna (Patch1) resonance frequency (f_r) is 1.291 THz, which is then decreased to 1.278 THz when the pure copper conducting layers are replaced using $G0$. Resonance is increased to 1.296 THz and 1.299 THz when the conducting materials are replaced by $G1$ and $G2$, respectively. This means that the resonance can be tuned by increasing or decreasing the chemical potential. The simulation results for the graphene-based antenna

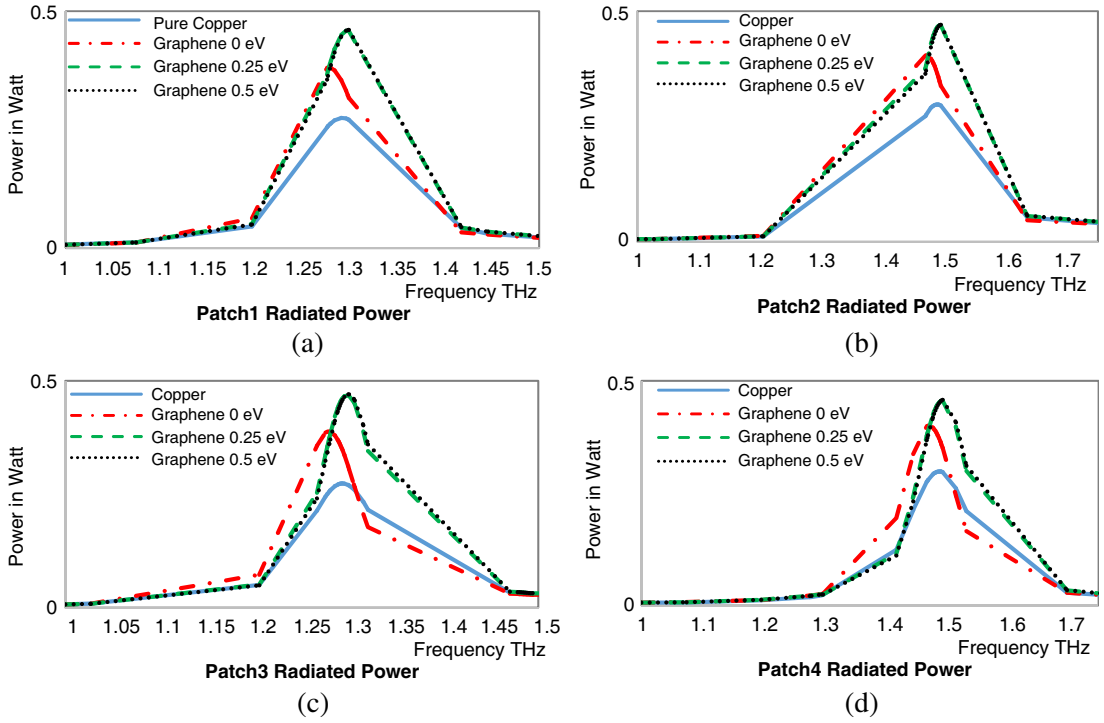

Figure 4. Radiated power for: (a) Patch1, (b) Patch2, (c) Patch3 and (d) Patch4. Legend: pure copper (solid blue line), $G1$ (red dashed dotted line), $G2$ (green dashed line) and $G3$ (black dotted line).

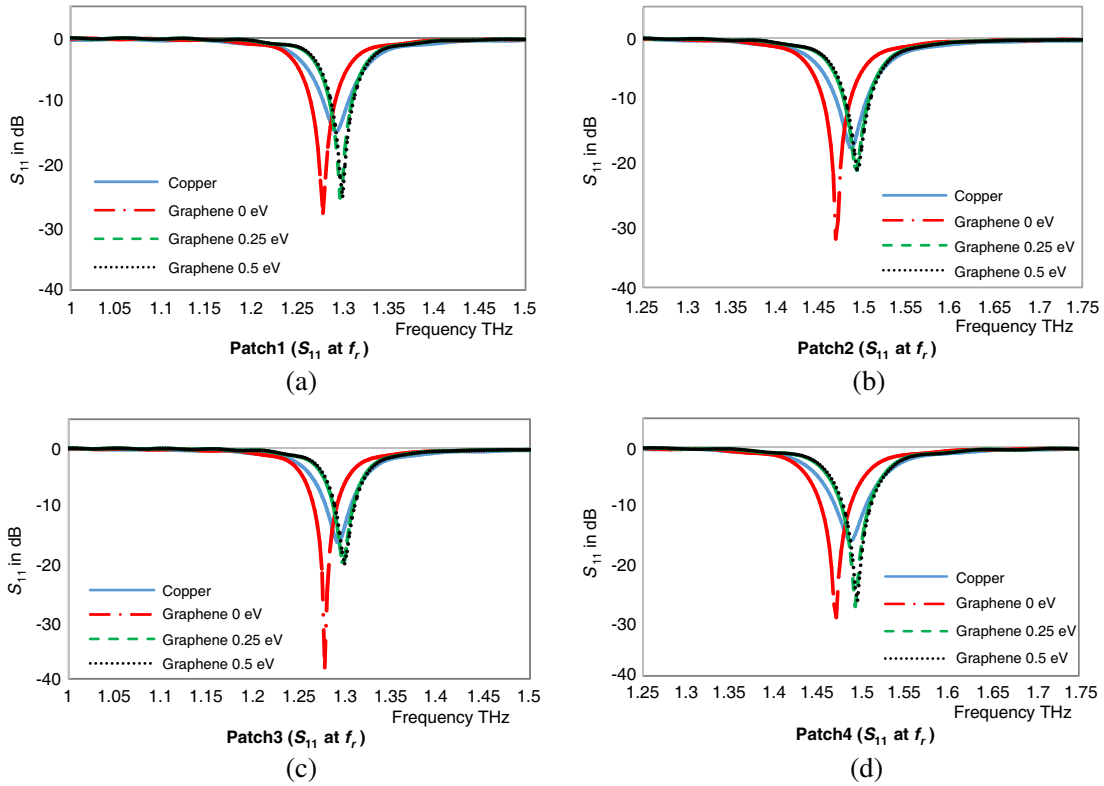

Figure 5. Reflection coefficients for: (a) Patch1, (b) Patch2, (c) Patch3, (d) Patch4. Legend: pure copper (solid blue line), $G1$ (red dashed dotted line), $G2$ (green dashed line) and $G3$ (black dotted line).

show a significant improvement over the copper based antenna in terms of reflection coefficient, high radiation efficiency and enhanced gain. Besides that, the slight improvement in directivity for the graphene-based patch antennas is also evident in this table. It is also observed from Table 3 that the performances of the elliptical graphene-based antennas for Patch2 and Patch3 are improved. This is similar to the behavior of the proposed rectangular patch (Patch1 and Patch4).

Both graphene-based elliptical patches showed better reflection coefficient, radiation efficiency and gain than the rectangular patch (Patch1). The minor improvements in these parameters of elliptical patch antenna are due to the higher surface area available on the elliptical patch than that of a rectangular patch when resonating similarly at 1.291 THz. On the other hand, the resonant frequency of the elliptical patch is higher than that of the rectangular patch when the dimensions (width and length) of the rectangular patch and substrate are the same as the major and minor axes of the elliptical patch. This is mainly due to the extended electrical length on the corners of the rectangular patch in comparison to the elliptical antenna. The elliptical patch also shows better radiation efficiency and gain than the rectangular patch at this resonance frequency. Figure 4 illustrates the improvement of the radiated power among the four patch antennas when the material of the two layers conducting element was changed. It is observed that the $G0$-based antenna (red dashed dotted line) radiated a higher power than pure copper based antenna (solid blue line). Besides that, antennas $G1$ and $G2$ (green dashed and black dotted lines, respectively) radiated more power than the previous two models. It can be concluded that the doped graphene with higher chemical potential produces higher radiated power. However, the difference between the radiated power for antennas $G1$ and $G2$ is small in comparison with pure copper and $G0$ based antennas.

Figure 5 illustrates the variation in the reflection coefficient for the four studied antennas when

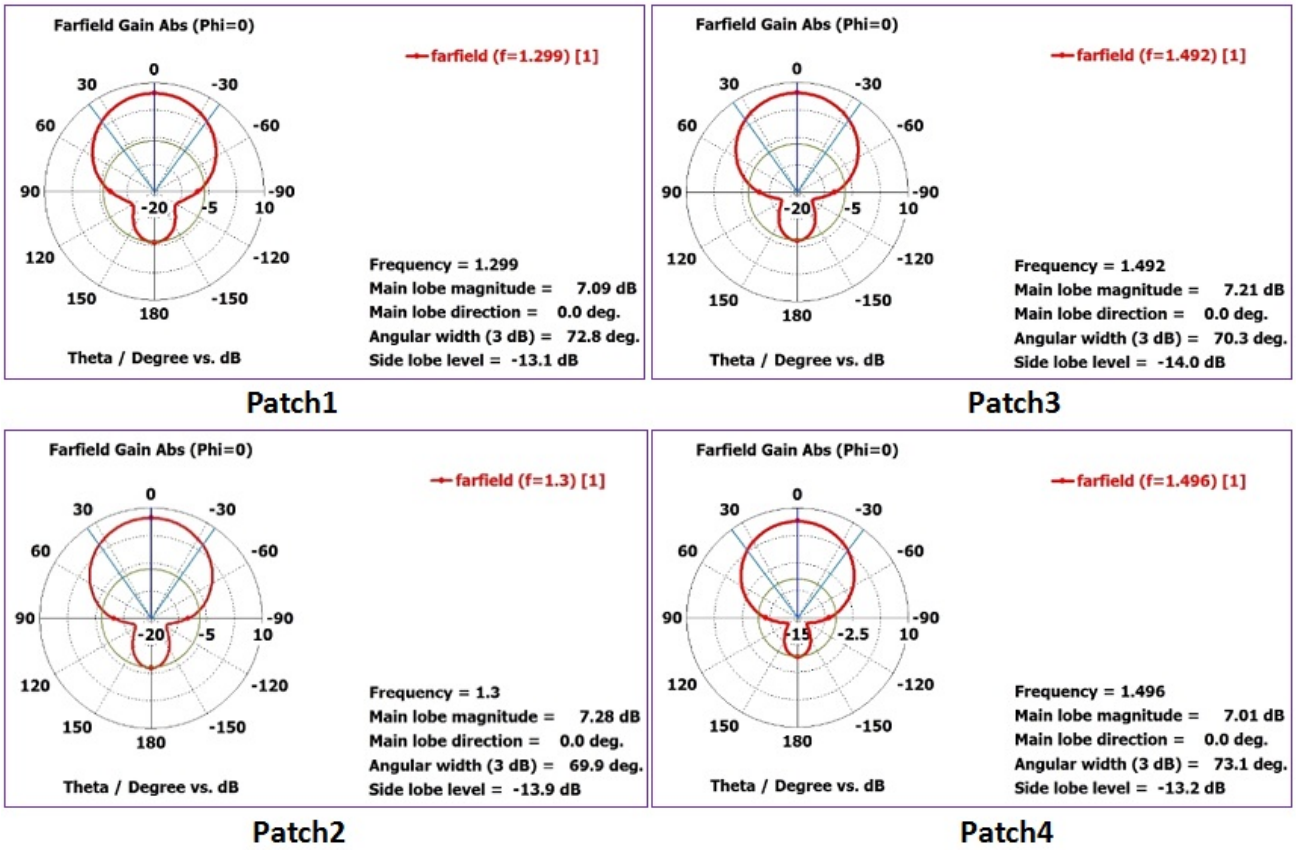

Figure 6. The far field radiation pattern of the four proposed doped graphene patch antennas: Elliptical patches (Patch-2 and Patch-3) features higher main lobe than that of rectangular patches at both frequencies.

Table 4. Comparison of the performance of the proposed antennas compared to previously investigated graphene based antenna reported in literature.

	f_r in THz	S_{11} at f_r in −dB	η_{rad} at f_r (%)	Dir at f_r in dB	Gain at f_r in dB
Ref. [23] at $\mu_c = 0.5\,\text{eV}$ (Yagi antenna)	2.86	15	NR	NR	6
Ref. [20] (strip dipole)	0.8	NR	20	0	NR
Ref. [14] (rectangular patch)	0.75	NR	86.58	5.71	5.09
Ref. [21] (rectangular patch)	6.0	39.37	37.17	7.56	3.27
Ref. [22] at $\mu_c = 0.5\,\text{eV}$ (triangular patch)	2.60	20.86	82.7	6.84	5.97
Proposed Patch3 at $\mu_c = 0.5\,\text{eV}$ (elliptical patch)	1.3	27.44	96	7.46	7.20
Proposed Patch2 at $\mu_c = 0.5\,\text{eV}$ (elliptical patch)	1.494	21.1	95	7.43	7.21

NR — not reported

biasing their conducting layers using different potentials. It shows that the reflection coefficient of the $G0$ graphene-based antenna is lowered compared to the pure copper based antenna. Besides that, a decrease in resonant frequency is also noticed. Note that $G1$ and $G2$ based antennas (which are approximately matched) have significant improvement for antenna reflection coefficients along with the increase of resonant frequencies compared to pure copper-based antennas. Antenna $G2$ resonates at higher frequency than $G1$, but the variation of resonance frequency between antennas $G1$ and $G2$ is small relative to the variations between pure copper antenna and antenna $G0$. This is due to the resulting graphene surface impedance with different values of chemical potential in this electromagnetic spectrum as shown in Figure 2. The conductivity of doped graphene in the mm wave and THz frequency bands is higher than that of non-doped graphene, resulting in lower surface impedance. Figure 6 shows far-field radiation patterns of the four proposed doped graphene-based patch antennas. The elliptical patches (Patch-2 and Patch-3) feature high main lobe magnitudes and lower side-lobe levels than the rectangular patches (Patch-1 and Patch-4) at resonance.

Table 4 compares the overall performance of the proposed elliptical patches against other previously studied graphene-based antennas. The proposed design shows the best improvements especially in terms of gain and radiation efficiency when doped graphene is used as its conducting elements.

5. CONCLUSIONS

The modeling and characterization of graphene-based antennas operating in the millimeter-wave and Terahertz bands have been presented. The modeling starts by numerically determining the surface impedance for a thin graphene layer using the Kubo formula. Next, these values are validated against two graphene-based microstrip antennas with different radiator topologies. The performance of the two antennas is determined by modeling and benchmarking them against their corresponding topology made using copper conductors in a commercial electromagnetic solver, CST Microwave Studio. The effect of different chemical potentials on the performance of both antennas is then studied by determining their surface properties (conductivities and impedances) prior to implementation and evaluation on these antennas. It is observed that the performance of the antenna with doped graphene as conducting elements indicates good improvements in terms of reflection coefficient, radiation efficiency, directivity and gain. For rectangular and elliptical antennas designed to resonate at two different frequencies

(1.291 THz and 1.488 THz), the latter consistently indicates better performance than the former. The gain and radiation efficiency improvements for the graphene-based elliptical patches when biased using small levels of voltages ($G1$ and $G2$) are also relatively higher than the prototype with copper conducting elements. Besides higher gain and radiation efficiency, it is also demonstrated that biasing enables the graphene-based antennas' resonance tuneability.

REFERENCES

1. Akyildiz, I. F., J. M. Jornet, and C. Han, "Terahertz band: Next frontier for wireless communications," *Physical Communication*, Vol. 12, 16–32, 2014.
2. Khiabani, N., "Modelling, design and characterisation of terahertz photoconductive antennas," Doctoral Thesis, University of Liverpool, 2013.
3. Huang, Y., N. Khiabani, Y. Shen, and D. Li, "Terahertz photoconductive antenna efficiency," *2011 International Workshop on Antenna Technology (iWAT)*, 152–156, 2011.
4. Danana, B., B. Choudhury, and R. M. Jha, "Design of high gain microstrip antenna for THz wireless communications," *International Journal of Advanced Research in Electrical, Electronics and Instrumentation Engineering*, Vol. 3, 711–716, 2014.
5. Llatser, I., C. Kremers, D. N. Chigrin, J. M. Jornet, M. C. Lemme, A. Cabellos-Aparicio, et al., "Radiation characteristics of tunable graphennas in the terahertz band," *Radioengineering*, Vol. 21, 946–953, 2012.
6. Niu, T., W. Withayachumnankul, B. S. Y. Ung, H. Menekse, M. Bhaskaran, S. Sriram, et al., "Reflectarray antennas for terahertz communications," arXiv preprint arXiv:1210.0653, 2012.
7. Hanson, G., "Radiation efficiency of nano-radius dipole antennas in the microwave and far-infrared regimes," *IEEE Antennas and Propagation Magazine*, Vol. 50, 66–77, 2008.
8. Walther, M., D. Cooke, C. Sherstan, M. Hajar, M. Freeman, and F. Hegmann, "Terahertz conductivity of thin gold films at the metal-insulator percolation transition," *Physical Review B*, Vol. 76, 125408, 2007.
9. Lacour, S. P., D. Chan, S. Wagner, T. Li, and Z. Suo, "Mechanisms of reversible stretchability of thin metal films on elastomeric substrates," *Applied Physics Letters*, Vol. 88, 204103, 2006.
10. Sharma, A. and G. Singh, "Rectangular microstirp patch antenna design at THz frequency for short distance wireless communication systems," *Journal of Infrared, Millimeter, and Terahertz Waves*, Vol. 30, 1–7, 2009.
11. Bayram, Y., Y. Zhou, B. S. Shim, S. Xu, J. Zhu, N. Kotov, et al., "E-textile conductors and polymer composites for conformal lightweight antennas," *IEEE Transactions on Antennas and Propagation*, Vol. 58, 2732–2736, 2010.
12. Deligeorgis, G., M. Dragoman, D. Neculoiu, D. Dragoman, G. Konstantinidis, A. Cismaru, et al., "Microwave propagation in graphene," *Applied Physics Letters*, Vol. 95, 073107, 2009.
13. Geim, A. K. and K. S. Novoselov, "The rise of graphene," *Nature Materials*, Vol. 6, 183–191, 2007.
14. Anand, S., D. S. Kumar, R. J. Wu, and M. Chavali, "Graphene nanoribbon based terahertz antenna on polyimide substrate," *Optik-International Journal for Light and Electron Optics*, Vol. 125, 5546–5549, 2014.
15. Akyildiz, I. F. and J. M. Jornet, "Electromagnetic wireless nanosensor networks," *Nano Communication Networks*, Vol. 1, 3–19, 2010.
16. Ju, L., B. Geng, J. Horng, C. Girit, M. Martin, Z. Hao, et al., "Graphene plasmonics for tunable terahertz metamaterials," *Nature Nanotechnology*, Vol. 6, 630–634, 2011.
17. Balanis, C. A., *Antenna Theory: Analysis and Design*, Vol. 1, John Wiley & Sons, 2005.
18. Wang, L., S. M. Uppuluri, E. X. Jin, and X. Xu, "Nanolithography using high transmission nanoscale bowtie apertures," *Nano Letters*, Vol. 6, 361–364, 2006.
19. Llatser, I., C. Kremers, A. Cabellos-Aparicio, J. M. Jornet, E. Alarcón, and D. N. Chigrin, "Graphene-based nano-patch antenna for terahertz radiation," *Photonics and Nanostructures-Fundamentals and Applications*, Vol. 10, 353–358, 2012.

20. Thampy, A. S., M. S. Darak, and S. K. Dhamodharan, "Analysis of graphene based optically transparent patch antenna for terahertz communications," *Physica E: Low-dimensional Systems and Nanostructures*, Vol. 66, 67–73, 2015.
21. Bala, R. and A. Marwaha, "Development of computational model for tunable characteristics of graphene based triangular patch antenna in THz regime," *Journal of Computational Electronics*, 1–6, 2015.
22. Tamagnone, M., J. S. Gomez-Diaz, J. R. Mosig, and J. Perruisseau-Carrier, "Reconfigurable terahertz plasmonic antenna concept using a graphene stack," *Applied Physics Letters*, Vol. 101, 214102, 2012.
23. Hanson, G. W., "Dyadic Green's functions for an anisotropic, non-local model of biased graphene," *IEEE Transactions on Antennas and Propagation*, Vol. 56, 747–757, 2008.
24. Gusynin, V. P., S. G. Sharapov, and J. P. Carbotte, "Magneto-optical conductivity in graphene," *Journal of Physics: Condensed Matter*, Vol. 19, 026222, 2006.
25. Radwan, A. H., M. D'Amico, and G. Gentili, "Reconfigurable THz Yagi antenna based on hybrid graphene-metal layout," *2014 Loughborough Antennas and Propagation Conference (LAPC)*, 671–675, 2014.
26. Costa, K., V. Dmitriev, C. Nascimento, and G. Silvano, "Graphene nanoantennas with different shapes," *2013 SBMO/IEEE MTT-S International Microwave & Optoelectronics Conference (IMOC)*, 1–5, 2013.